UBVI Surface Photometry of the Spiral Galaxy NGC 300 in the Sculptor Group

Sang Chul Kim[1], Hwankyung Sung[2], Hong Soo Park[3] and Eon-Chang Sung[1]

[1] Korea Astronomy Observatory, Taejon 305-348, Republic of Korea; sckim@kao.re.kr
[2] Department of Astronomy and Space Science, Sejong University, 98 Gunja-dong, Gwangjin-gu, Seoul 143-747, Republic of Korea
[3] Astronomy Program, SEES, Seoul National University, Seoul 151-742, Republic of Korea

Abstract   We present *UBVI* surface photometry over a $20.5' \times 20.5'$ area of the late-type spiral galaxy NGC 300. We have derived isophotal maps, surface brightness profiles, ellipticity profiles, position angle profiles, and color profiles. By merging our *I*-band measurements with those of Böker et al. based on *Hubble Space Telescope* observations, we have obtained combined *I*-band surface brightness profiles for the region $0.02'' < r < 500''$ and have decomposed the profiles into three components: a nucleus, a bulge, and an exponential disk.

Key words: galaxies: spiral — galaxies: photometry — galaxies: individual (NGC 300) — galaxies: nuclei

1   INTRODUCTION

NGC 300 (=ESO 295–G020, IRAS 00525–3757, PGC 3238) is a late-type (SA(s)d, de Vaucouleurs et al. 1991) spiral galaxy in the nearest galaxy group, the Sculptor Group, which consists of five major spiral galaxies (NGC 55, NGC 247, NGC 253, NGC 300, and NGC 7793) and ∼20 dwarf galaxies (Côté et al. 1997; Whiting 1999; Karachentsev et al. 2003; cf. van den Bergh 1999). NGC300 is a rather bright ($M_B = -18.6$) and nearly face-on galaxy, similar to M33 in the northern hemisphere (Blair & Long 1997). Some basic information of this galaxy is summarized in Table 1, which supplements the table 1 of Kim, Sung & Lee (2002, hereafter Paper I).

Although there have been several studies on various objects in NGC 300 (e.g., Paper I and references therein), only a few are dedicated to surface photometry. De Vaucouleurs & Page (1962) made such a study using photographic plates obtained by the Mount Stromlo 30- and 74-inch reflectors. Carignan (1985) carried out surface photometry of three Sculptor group galaxies including NGC 300. He used B_J-band photographic plates taken with the 1.2m Schmidt telescope of Siding Spring Observatory. Recently, Böker et al. (2002, 2004) observed 77 nearby late-type spiral galaxies including NGC 300 using the *Hubble Space Telescope (HST)*/WFPC2. They used the *I*-band images of the galaxies to study the nuclear star clusters and identified distinct, compact, and dominant sources at, or very close to, the photocenters. For NGC 300, they presented the *I*-band surface brightness profile inside $r \sim 15''$ and photometric parameters of the nuclear star cluster.

Table 1 Basic Information on NGC 300

Parameter	Information	Reference
$\alpha_{\rm J2000}, \delta_{\rm J2000}$	$0^{\rm h}54^{\rm m}53.48^{\rm s}, -37^\circ 41' \, 03.8''$	[1]
l, b	$299.21^\circ, -79.42^\circ$	[1]
Type	SA(s)d	[2]
HI heliocentric radial velocity, $v_\odot$	142 ± 4 km s^{-1}	[2]
Maximum rotational velocity, $V_{\rm max}$	87 km s^{-1}	[3]
Foreground reddening, $E(B-V)$	0.013 mag	[4]
Isophotal major diameter at the 25.0 B mag arcsec^{-2} level, D_{25}	$21.9'$	[2]
Position angle	111°	[2]
Minor to major axis ratio at D_{25}, $(b/a)_{25}$	0.74	[3]
Inclination i	$42.3^\circ \pm 3.0^\circ$	[3]
Distance modulus, $(m-M)_0$	26.53 ± 0.07 mag	[5]
Distance, d	2.02 ± 0.07 Mpc ($1'' = 9.8$ pc)	[5]
Exponential disk corrected central surface brightness, $\mu_B(0)$	22.23 mag arcsec^{-2}	[3]
Exponential disk corrected central surface brightness, $\mu_I(0)$	19.97 mag arcsec^{-2}	This study
Scale length, r_s (obtained from B-band)	2.06 kpc	[3]
Scale length, r_s (obtained from I-band)	1.47 kpc	This study
Apparent total magnitude, $B_{\rm T}$	8.72 ± 0.05 mag	[2]
Apparent total color index, $(B-V)_{\rm T}$	0.59 ± 0.03 mag	[2]
Apparent total color index, $(U-B)_{\rm T}$	0.11 ± 0.03 mag	[2]
Corrected total magnitude, $B_{\rm T}^0$	8.53	[2]
Corrected total color index, $(B-V)_{\rm T}^0$	0.56	[2]
Corrected total color index, $(U-B)_{\rm T}^0$	0.09	[2]
Absolute total magnitude, M_{B_T}	-18.59	[6]
Metallicity from the ratio of carbon stars to M stars of spectral type M5 or later, [Fe/H]	-0.5 dex	[7]
HI column density in the direction of NGC 300	2.97×10^{20} atoms cm^{-2}	[8]
HI flux	≤ 670 Jy km s^{-1}	[3]
HI mass, $M_{\rm HI}$	$(2.5 \pm 0.1) \times 10^9$ $M_\odot$	[9]

Note: [1] NASA/IPAC Extragalactic Database; [2] de Vaucouleurs et al. 1991; [3] Carignan 1985; [4] Schlegel et al. 1998; [5] Freedman et al. 2001 (cf. Butler et al. 2004); [6] Sandage & Tammann 1981; [7] Richer, Pritchet & Crabtree 1985; [8] Read, Ponman & Strickland 1997; [9] Rogstad, Crutcher & Chu 1979.

So far there has not been any surface photometry study of NGC 300 with multi-band filters and CCD imaging. In this paper, we present surface photometry based on $UBVI$ CCD images of a $20.5' \times 20.5'$ area of NGC 300 and we have derived the surface brightness and color distributions, and structural parameters for an $r < 500''$ region. This paper is organised as follows: Sect. 2 describes the photometric observations and the data reduction process. Sect. 3 gives the Isophotal maps, Sect. 4, the ellipse fitting results, and Sect. 5, the profiles in the colors. In Sect. 6 we compare our results of surface photometry with previous results and present the results of decomposing the surface brightness profile into three components. Finally, a brief summary is given in Sect. 7.

2   OBSERVATIONS AND DATA REDUCTION

$UBVI$ CCD photometry was carried out on 1997 November 23 at Siding Spring Observatory with the 40 inch (1m) telescope (f/8) and a thinned SITe 2048×2048 CCD (24μm pixels). The scale was $0.602''$ pixel^{-1}, giving $20.5'$ each side. The exposure time used was 1200s in U, 600s in B, 300s in V, and 120s in I. The night was photometric and the seeing was $1.5''$ in U, $1.6''$ in B, $1.4''$ in V and $1.4''$ in I.

All the preprocessing, such as overscan correction, bias subtraction and flat fielding was done using the IRAF*/CCDRED package. The surface photometry from the CCD images was carried out using the ellipse fitting task IRAF/SPIRAL (Surface Photometry Interactive Reduction and Analysis Library), a package developed at Kiso Observatory for galaxy surface photometry (Ichikawa et al. 1987) which is essentially the same as that described by Kent (1983). Smoothing of the images was done using variable-width Gaussian beam of the IRAF/SPIRAL.SMOOTH task to improve the signal-to-noise ratio in the outer regions of the galaxy.

The instrumental magnitudes were transformed to the standard Johnson-Cousins $UBVI$ system using the equatorial standards of South African Astronomical Observatory (SAAO) (Menzies et al. 1991) and blue and red standards of Kilkenny et al. (1998), both observed on the same night. The atmospheric extinction coefficients were determined from the photometry of standard stars using the transformation coefficients adopted by Sung & Bessell (2000). The transformation equations we derived from the photometry of the standard stars are $u = U + 4.987 + 0.545 \times X_u + u3 \times (U - B)$, $b = B + 2.542 + 0.289 \times X_b + 0.101 \times (B - V)$, $v = V + 2.412 + 0.147 \times X_v - 0.072 \times (B - V)$, and $i = I + 2.869 + 0.090 \times X_i - 0.028 \times (V - I)$, where lowercase and uppercase letters represent, respectively, the instrumental system and standard system (zeropoint= 25.0), X is the air mass and $u3$ is -0.006 when $(U - B) \geq 0.0$ and -0.125 when $(U - B) < 0.0$. The rms scatter of the standard stars was 0.012 mag in U, 0.008 mag in B, 0.011 mag in V, and 0.015 mag in I, indicating the good photometric quality on the night.

The sky background was determined from the mode values of the south-east edges of the images which are the farthest clear regions from the galaxy (the distance from the center of NGC 300 is $\sim 800''$). These values were subtracted from the individual images. We calculated the surface brightnesses for these sky values, obtaining 21.59 ± 0.22 mag arcsec^{-2} for U, 22.33 ± 0.08 for B, 21.58 ± 0.07 for V, and 19.04 ± 0.03 for I. The errors quoted here are the estimated standard deviations. Considering that at the time of the observation the moon was 23 days old (or 7 days before the next new Moon) and that the air-mass of our target is in the range of 1.00–1.02, our sky brightness estimates seem to be reasonably similar to those of the Kitt Peak National Observatory (Elias 1994; Kim, Lee & Geisler 2000) or to those of the Crimea/Hawaii sites (Leinert et al. 1995).

3 MORPHOLOGICAL CHARACTERISTICS OF NGC 300

Greyscale maps of B and V CCD images of NGC 300 are shown in Figs. 1a and 1b (size $20.5' \times 20.5'$). Most of the brightest stars in the images are foreground stars. The B-band image in Fig. 1a shows the spiral features well, manifesting several lumps of bright stars that are stellar associations (Pietrzyński et al. 2001, Paper I). The central region shown in Fig. 1b reveals that the bulge of this SA(s)d type galaxy is quite small compared to the size of the spiral arms; this feature will be discussed in Sect. 6.2.

Figure 2 shows isophotal maps of NGC 300 (contour interval 0.5 mag arcsec^{-2}). Axes are in pixel units; tick marks at intervals of $60.2''$. No conspicuous bulges are seen in the isophotes which are elongated in the NW-SE direction excepting the innermost one. Even though the eastern spiral arm is clearly seen in both panels of Fig. 2, the (north-)western arm is barely delineated here due to the large association of bright stars around $(X = 1750, Y = 100)$. These two major arms are those noted by Sandage & Bedke (1994).

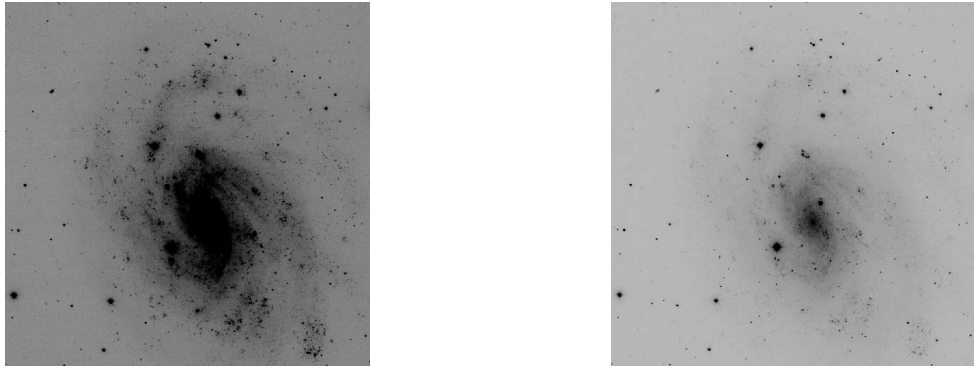
Fig. 1   CCD images of NGC 300.   North is to the right, east is at the top.   The scale is
0.602″ pixel^{-1} and the size of the field is 20.5′ × 20.5′. (a: left panel) A greyscale image in the
B band. The spiral arms are easily seen here. (b: right panel) The same in the V band. This
figure shows the central region of the galaxy with faint traces of spiral arms. In both panels,
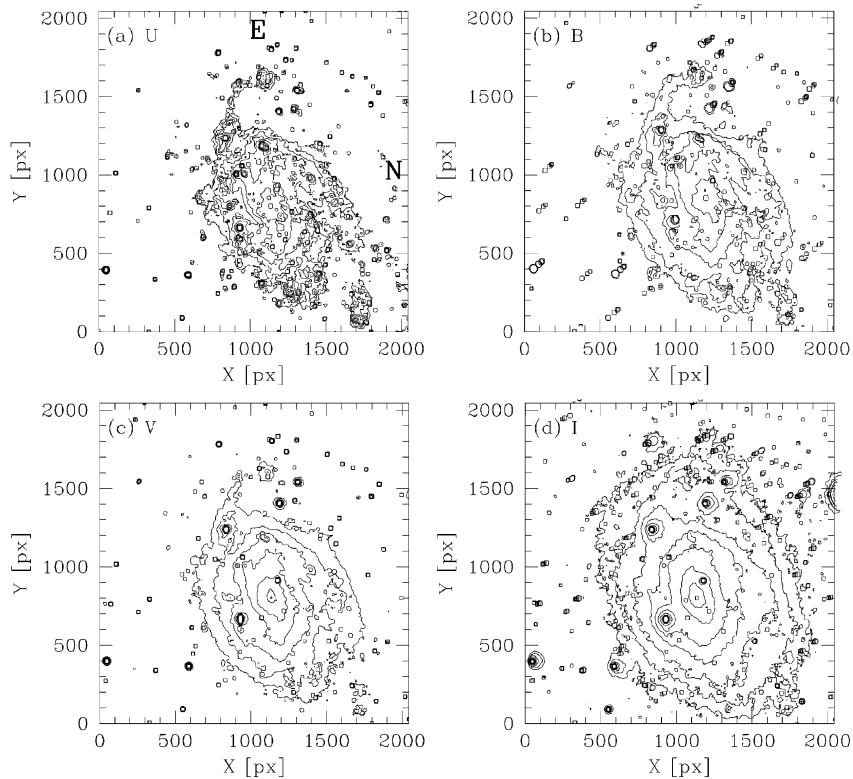the brightest stars are mostly foreground stars.

Fig. 2   Isophotal contour maps of NGC 300 in the U-band (a), B-band (b), V-band (c), and
I-band (d). North is to the right, and east is at the top. Size of each field 20.5′ × 20.5′, 60.2″
between the ticks. Contour interval 0.5 mag arcsec^{-2}.

4   ELLIPSE FITTING

We have applied the ellipse fitting task IRAF/SPIRAL.PROFS.VPROF to the NGC 300 images to obtain the surface brightness profiles as well as the ellipticity (ϵ) and position angle (PA) profiles.

Figure 3 shows the radial surface brightness profiles along the major axis for the region $r < 500''$. Typical errors in B and V are indicated in the lower and upper panels, respectively. Since the IRAF/SPIRAL task does not give the error of the surface brightness, we evaluated the error using the IRAF/STSDAS.ANALYSIS.ISOPHOTE.ELLIPSE task at the given radius for the ellipticity, position angle, and center coordinates obtained from the SPIRAL task. Unlike the elliptical galaxies which have smooth brightness profiles, spiral galaxies are patchy and have spiral arm features. The local patchy features led to the non-systematic error values in Fig. 3, though the low photon signals relative to the sky brightness made the errors to increase at the outer radii.

The U and B surface brightness profiles are very similar in their values, which can be deduced from the apparent total $(U - B)$ color index of 0.11 ± 0.03 mag (de Vaucouleurs et al. 1991). While the U surface brightnesses are fainter than the B values at $r < 200''$, they get brighter at $r > 200''$.
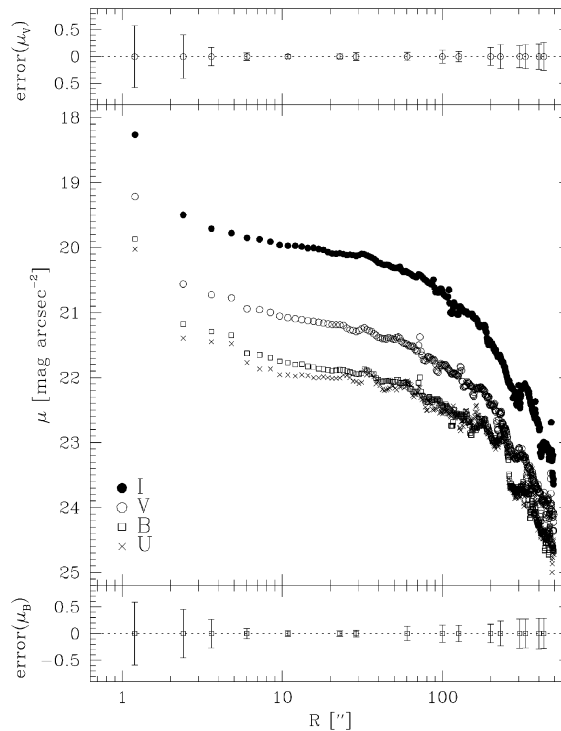

Fig. 3 U, B, V, and I major axis surface brightness profiles of NGC 300. The typical errors of B and V-band surface brightnesses are indicated in the lower and upper panels, respectively. *The data are available from one of the authors (S.C.K.).*

Figure 4 shows the ellipticity ($\epsilon = 1 - b/a$, a and b being the semi-major and semi-minor axis lengths, respectively) profiles of NGC 300 in the four bands. The straight lines are fits by the eye and are the same for all the bands. The ellipticity increases from ~ 0 at $r \sim 2''$ to ~ 0.5 at $r \sim 200''$, and then decreases further out. The amplitude of its variation is rather larger in the U- and B-bands than in the V- and I-bands, and so are the absolute values of the ellipticity at $r > 100''$.
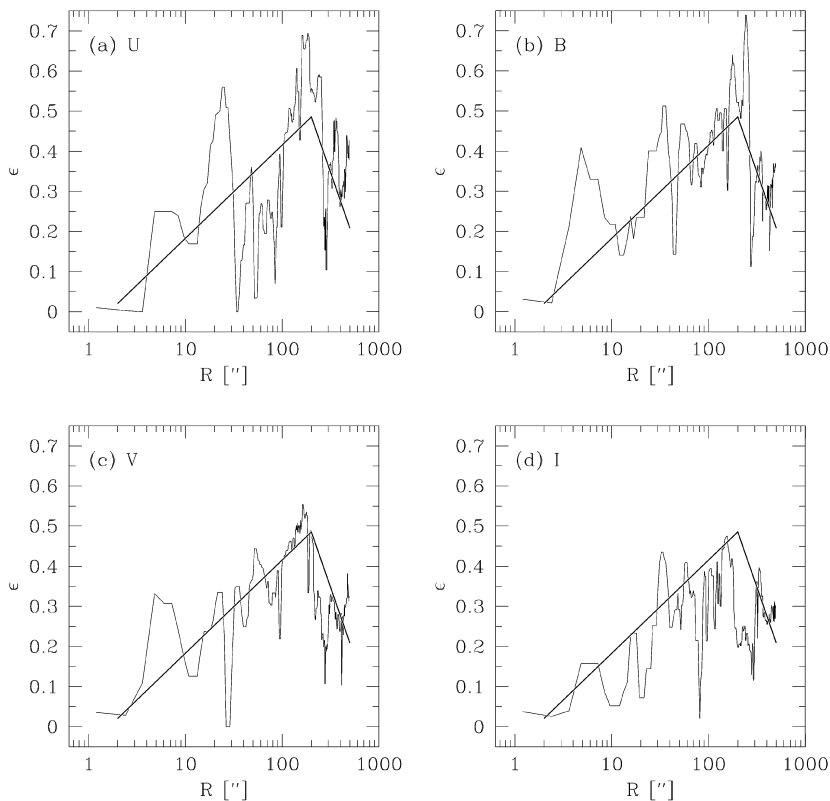

Fig. 4   Ellipticity profiles of NGC 300. The straight lines are eye-fits and are the same for all bands.

Figure 5 shows the position angle (PA; N through E to the major axis) profiles of NGC 300 in the four bands. The straight lines are eye-fits and are the same for all the four bands. The position angle increases from $\sim 40°$ at $r \sim 1''$ to $2''$ to $\sim 110°$ at $r \sim 40''$, and fluctuates around $\sim 110°$ at $r > 40''$. This PA value of $\sim 110°$ is in good agreement with those obtained by Carignan (1985, $105.6° \pm 1.8°$) and by de Vaucouleurs et al. (1991, $111°$). The changes in the position angle are mainly due to the spiral structure and there is no region where the PA is flat (which is an indicator of a bar structure, Choi et al. 1998).
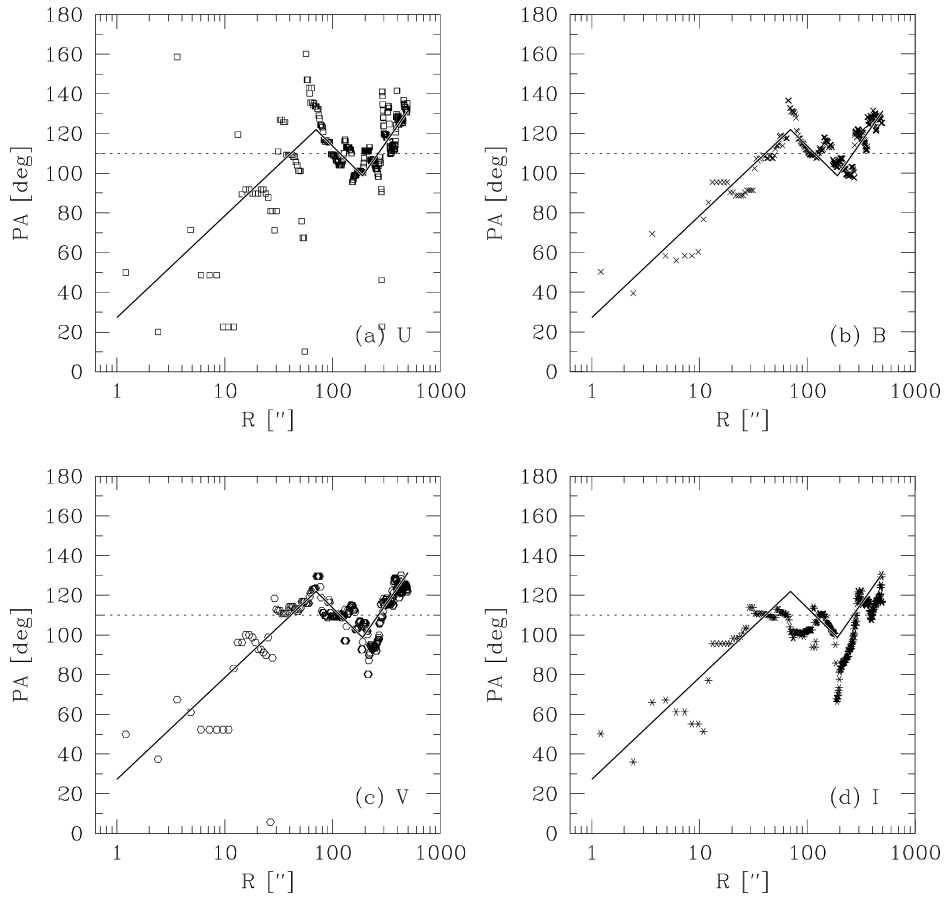
Fig. 5   Position angle profiles of NGC 300. The straight lines are eye-fits and are the same for all the four bands.

5   COLOR PROFILES

Figure 6 shows the surface color profiles of NGC 300 along the major axis. Here surface color means the differential color per square arcsecond. The errors for the $(B - V)$ color are plotted in the upper panel to show the typical size of error. The solid lines are least-square fits to the data; they yield a gradient of -0.07 mag arcsec^{-2} $(100'')^{-1}$ for $(U - B)$, of -0.11 mag arcsec^{-2} $(100'')^{-1}$ for $(U - V)$, of -0.14 mag arcsec^{-2} $(100'')^{-1}$ for $(U - I)$, of -0.04 mag arcsec^{-2} $(100'')^{-1}$ for $(B - V)$, of -0.07 mag arcsec^{-2} $(100'')^{-1}$ for $(B - I)$, and of -0.04 mag arcsec^{-2} $(100'')^{-1}$ for $(V - I)$. As the wavelength separation between the filters gets larger, the slope gets steeper: the steepest slope is in the $(U - I)$ color, and the least steep slopes are in the $(B - V)$ and $(V - I)$ colors.

NGC 300 shows typical color profiles of late-type spiral galaxies, being redder in the inner regions and getting bluer as the radius increases. The primary factor for this negative radial color gradient is the difference in the underlying stellar populations between the inner and outer parts of the galaxies (Kim & Ann 1990).
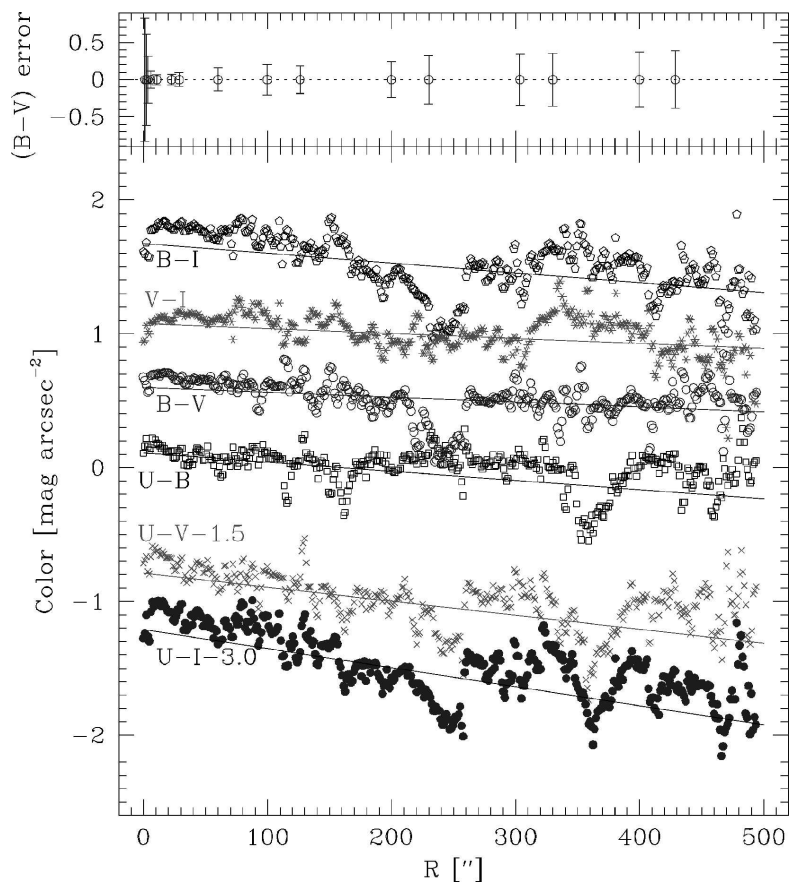
Fig. 6   Radial surface color profiles of NGC 300. The errors for the $(B - V)$ color are plotted in the upper panel to show the typical error values.

6   DISCUSSION

6.1   Comparison with Previous Studies

Figure 7 compares the surface brightness profiles obtained in this study with those given by previous studies. The radius scale is logarithmic in Fig. 7a and linear in Fig. 7b. Both de Vaucouleurs & Page (1962) and Carignan (1985) have given B-band surface brightness profiles obtained from photographic plates; these are drawn as dashed lines and dotted lines (equivalent profile) or open triangles (elliptically averaged profile), respectively. B_J magnitudes of Carignan (1985) are transformed to B magnitudes using the relation $B = B_J + 0.06(B_J - R_F) = B_J + 0.05$ (Carignan 1985). The recent HST-based I-band surface brightness profiles for the inner $r < 15''$ region of NGC 300 given by Böker et al. (2002) are drawn in solid lines. Because the Böker et al.'s I-band surface brightnesses are $0.58 \, \mathrm{mag \, arcsec^{-2}}$ brighter than those in this study, we have added $0.58 \, \mathrm{mag \, arcsec^{-2}}$ to their values.
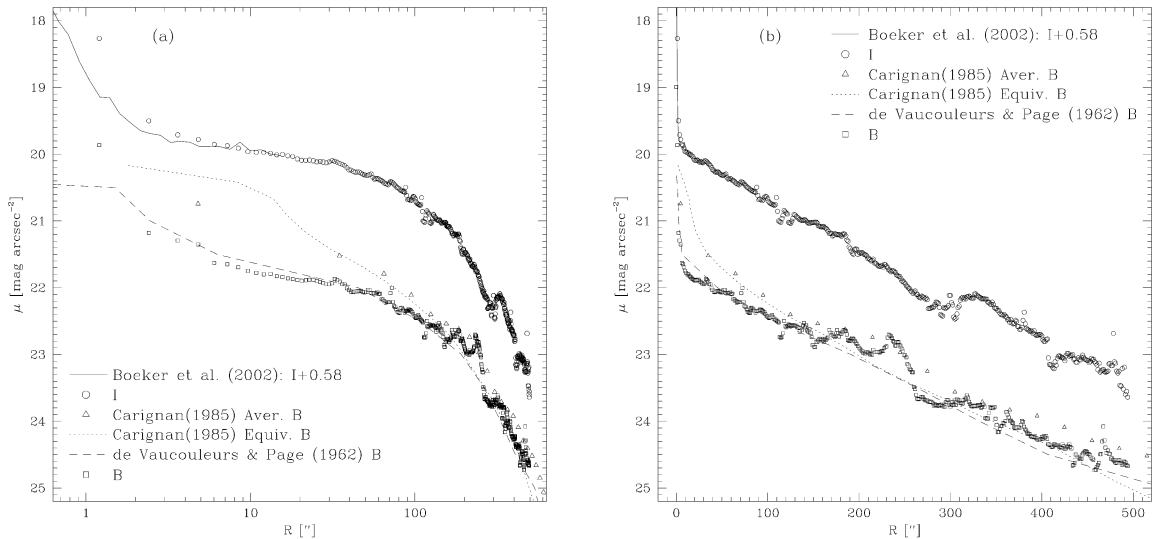
Fig. 7 Comparison of the surface brightness profiles obtained in this study with those of previous studies on logarithmic radius scale (panel a) and linear radius scale (panel b). B and I surface brightnesses obtained in this study are marked as open squares and open circles, respectively. B_J magnitudes of Carignan (1985) are transformed to B magnitudes using the relation $B = B_J + 0.06(B_J - R_F) = B_J + 0.05$ (Carignan 1985); $0.58\,\mathrm{mag\ arcsec^{-2}}$ is systematically added to the Böker et al. (2002)'s I-band surface brightnesses to match their profiles to those obtained in this study.

For the B-band surface brightness profiles, our profiles are in good agreement with those of de Vaucouleurs & Page (1962) for $r \lesssim 160''$ and with the equivalent profiles of Carignan (1985) in the outer region. Carignan (1985) noted the differences between his and de Vaucouleurs & Page (1962)'s profiles up to $0.4\,\mathrm{mag\ arcsec^{-2}}$ and being larger in the central region. This difference between these two studies seems to be due to some problems in the density-to-intensity calibration of the photographic plates since both studies are based on photographic plate photometry.

The I-band surface brightness profiles of NGC 300 given by Böker et al. (2002) are $\sim 0.6\,\mathrm{mag}$ $\mathrm{arcsec^{-2}}$ brighter than those in our study. Since Böker et al. observed their galaxies with the F814W filter only, they made the photometric calibration and conversion to Johnson's I-band assuming a standard color of $V - I = 1$ for all the galaxies. Nevertheless, this does not account for the rather large difference between the two photometric studies, because even 1 mag of change in the color of a galaxy gives only ~ 0.01 mag difference in the zero-point as they quoted. Apart from the zero-point difference between the two studies and some discrepancies at a few central points, the two I-band surface brightnesses show reasonable agreement especially for $r > 5''$. For the very central region of $r < 5''$, Böker et al. (2002)'s results based on the HST high-resolution CCD images should be considered as reliable.

6.2 Surface Brightness Profile Decomposition

We have combined our I-band surface brightness measurements for the region $r > 5''$ with those of Böker et al. (2002) for the region between $0.02''$ and $5''$. The combined profile is

shown in Fig. 8 as open circles. Using this combined surface brightness profile for the region of $0.02'' < r < 500''$, we have performed a three-component decomposition into a nucleus, a bulge and a disk (Stephens & Frogel 2002). We assume an exponential disk

$$I_{\text{disk}}(r) = I_0 \, \exp\frac{-r}{R_d} \qquad (1)$$

with central intensity I_0 and disk scale length R_d, and a de Vaucouleurs $r^{1/4}$ bulge

$$I_{\text{bulge}}(r) = I_e \, \exp\{-7.67 \, [(\frac{ar}{R_e})^{1/4} - 1]\} \qquad (2)$$

with an effective radius R_e and an intensity I_e at R_e. The factor $a = [(1 + \cos^2 i)/2]^{1/2}$ is a correction factor for deprojecting a spherical bulge, and an inclination of $i = 42.3°$ (Carignan 1985) is used. For the core component, we have used Sersic's model (Sersic 1968)

$$I_{\text{core}}(r) = I_s \, \exp\Big\{ - b_n \Big[\Big(\frac{ar}{R_s}\Big)^{1/n} - 1\Big]\Big\}, \qquad (3)$$

where R_s is an effective radius, I_s is the intensity at R_s, and n is the shape index ($b_n \approx 1.9992n - 0.3271$). The result of the three-component decomposition is shown in Fig. 8, and the parameter values are listed in Table 2. Figure 8 shows that NGC 300 has a central peak in the surface brightness at $r < 1''$ which is reasonably fitted by the Sersic function, a disk with a central surface brightness of $19.97 \, \text{mag arcsec}^{-2}$ and scale length of $R_d = 2.5' \, (= 1.47 \, \text{kpc})$, and a very faint spheroidal component which is even fainter than that of M33 (Stephens & Frogel 2002).

Table 2   Model Parameters for the I-band Three-Component Decomposition

	Parameter	Value
Disk	scale length, R_d	$150'' = 2.50' = 1.47 \, \text{kpc}$[a]
	central surface brightness, μ_0	$19.97 \, \text{mag arcsec}^{-2}$
Bulge	effective radius, R_e	$1900'' = 31.67' = 18.62 \, \text{kpc}$[a]
	surface brightness at R_e, μ_e	$29.25 \, \text{mag arcsec}^{-2}$
Core	effective radius, R_s	$0.094'' = 0.92 \, \text{pc}$[a]
	surface brightness at R_s, μ_s	$16.55 \, \text{mag arcsec}^{-2}$
	shape index, n	1.43

Note: [a] Assuming the distance modulus of $(m - M)_0 = 26.53 \pm 0.07 \, \text{mag}$ (Freedman et al. 2001), which gives $1'' = 9.8 \, \text{pc}$.

The nuclear star cluster observed by Böker et al. (2002) using the *HST* has been included in the globular cluster candidate catalogue of Paper I with highest probability. It would be helpful to make a spectroscopic observation of this nuclear star cluster of NGC 300 to confirm the suggestion of Soffner et al. (1996) that the nucleus is an unresolved compact stellar cluster and to understand its nature. Information on the velocity dispersion of this object will also give a clue on the existence of any black hole in it (Gebhardt et al. 2001; Gebhardt, Rich & Ho 2002).

More surface brightness data in other passbands at high spatial resolution will be valuable to obtain information on the existence of any color gradient in the nuclear region of NGC 300 (Kormendy & McClure 1993; Kim & Lee 1998).
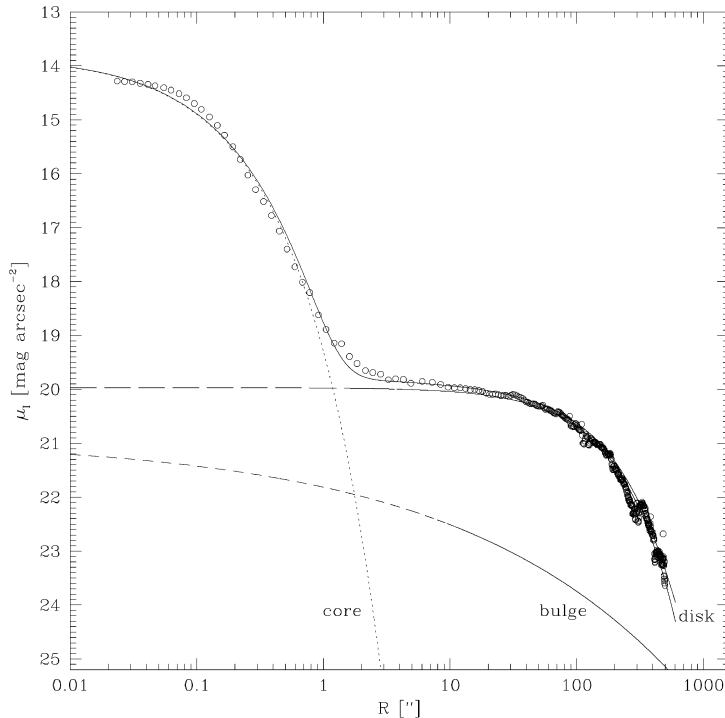
Fig. 8 Profile decomposition of the *I*-band surface brightness profile obtained in this study (for $r > 5''$) combined with measurements from Böker et al. (2002, $0.02'' < r < 5''$). The open circles are the observed data points, and the results of a three-component decomposition are an exponential disk (*long-dashed line*), an $r^{1/4}$ bulge (*short-dashed line*) and a Sersic core (*dotted line*). The solid line is the combined result of the three components.

7 SUMMARY

We have presented surface photometry for a $20.5' \times 20.5'$ area of the SA(s)d galaxy NGC 300 in the Sculptor group. We derived the isophotal maps, surface brightness profiles, ellipticity profiles, position angle profiles and color profiles. We have decomposed the *I*-band surface brightness profiles of the $0.02'' < r < 500''$ region into a nucleus, a bulge and an exponential disk.

References

Blair W. P., Long K. S., 1997, ApJS, 108, 261

Böker T., Laine S., van der Marel R. P. et al., 2002, AJ, 123, 1389

Böker T., Sarzi M., McLaughlin D. E., van der Marel R. P., Rix H.-W., Ho L. C., Shields J. C., 2004, AJ, 127, 105

Butler D. J., Martínez-Delgado D., Brander W., 2004, AJ, 127, 1472

Carignan C., 1985, ApJS, 58, 107

Choi Y.-J., Park B.-G., Yoon T. S., Ann H. B., 1998, Jour. of the Korean Astron. Soc., 31, 141

Côté S., Freeman K. C., Carignan C., Quinn P. J., 1997, AJ, 114, 1313

de Vaucouleurs G., Page J., 1962, ApJ, 136, 107

de Vaucouleurs G., de Vaucouleurs A., Corwin H. G., Jr. et al., 1991, Third Reference Catalogue of Bright Galaxies, New York: Springer-Verlag (RC3)

Elias J., 1994, NOAO Newsletter, No. 37, 1

Freedman W. L., et al., 2001, ApJ, 553, 47

Gebhardt K., et al., 2001, AJ, 122, 2469

Gebhardt K., Rich R. M., Ho L. C., 2002, ApJ, 578, L41

Ichikawa S., Okamura S., Watanabe M. et al., 1987, Annals Tokyo Astron. Obs., 21, 285

Karachentsev I. D., Grebel E. K., Sharina M. E. et al., 2003, A&A, 404, 93

Kent S. M., 1983, ApJ, 266, 562

Kilkenny D., van Wyk F., Roberts G. et al., 1998, MNRAS, 294, 93

Kim E., Lee M. G., Geisler D., 2000, MNRAS, 314, 307

Kim K. O., Ann H. B., 1990, Jour. of the Korean Astron. Soc., 22, 43

Kim S. C., Lee M. G., 1998, Jour. of the Korean Astron. Soc., 31, 51

Kim S. C., Sung H., Lee M. G., 2002, Jour. of the Korean Astron. Soc., 35, 9 (Paper I)

Kormendy J., McClure R. D., 1993, AJ, 105, 1793

Leinert Ch., Väisänen P., Mattila K., Lehtinen K., 1995, A&AS, 112, 99

Menzies J., Marang F., Laing J. D. et al., 1991, MNRAS, 248, 642

Pietrzyński G., Gieren W., Fouqué P., Pont F., 2001, A&A, 371, 497

Read A. M., Ponman T. J., Strickland D. K., 1997, MNRAS, 286, 626

Richer H. B., Pritchet C. J., Crabtree D. R., 1985, ApJ, 298, 240

Rogstad D. H., Crutcher R. M., Chu K., 1979, ApJ, 229, 509

Sandage A., Bedke J., 1994, The Carnegie Atlas of Galaxies, Washington, D. C.: Carnegie Institution of Washington

Sandage A. R., Tammann G. A., 1981, A Revised Shapley-Ames Catalog of Bright Galaxies, Washington, D. C.: Carnegie Institution of Washington

Schlegel D., Finkbeiner D., Davis M., 1998, ApJ, 500, 525

Sersic J. L., 1968, Atlas de Galaxias Australes, Córdoba: Observatorio Astronómico

Soffner T., Méndez R. H., Jacoby G. H. et al., 1996, A&A, 306, 9

Stephens A. W., Frogel J. A., 2002, AJ, 124, 2023

Sung H., Bessell M. S., 2000, PASA, 17, 244

van den Bergh S., 1999, ApJ, 517, L97

Whiting A. B., 1999, AJ, 117, 202